

Collect-and-Distribute Transformer for 3D Point Cloud Analysis

Haibo Qiu, Baosheng Yu, Dacheng Tao

School of Computer Science, The University of Sydney, Australia
 {hqiu2518, baosheng.yu, dacheng.tao}@sydney.edu.au

Abstract

Although remarkable advancements have been made recently in point cloud analysis through the exploration of transformer architecture, it remains challenging to effectively learn local and global structures within point clouds. In this paper, we propose a new transformer architecture equipped with a collect-and-distribute mechanism to communicate short- and long-range contexts of point clouds, which we refer to as CDFormer. Specifically, we first utilize self-attention to capture short-range interactions within each local patch, and the updated local features are then collected into a set of proxy reference points from which we can extract long-range contexts. Afterward, we distribute the learned long-range contexts back to local points via cross-attention. To address the position clues for short- and long-range contexts, we also introduce context-aware position encoding to facilitate position-aware communications between points. We perform experiments on four popular point cloud datasets, namely ModelNet40, ScanObjectNN, S3DIS, and ShapeNetPart, for classification and segmentation. Results show the effectiveness of the proposed CDFormer, delivering several new state-of-the-art performances on point cloud classification and segmentation tasks. The code is available at <https://github.com/haibo-qiu/CDFormer>.

1 Introduction

Point clouds have been extensively investigated in recent years, mainly due to their numerous promising real-world applications, such as autonomous driving [2, 32] and robotics [29, 68]. Unlike 2D images, a point cloud is a set of 3D points distributed in an irregular and disordered manner, where each point is mainly characterized by its Cartesian coordinates (x, y, z) . These fundamental differences make it non-trivial to utilize off-the-shelf 2D deep architectures for point cloud analysis. Therefore, many recent methods have developed different deep architectures to handle the special characteristics of point clouds, including mlp-based [37, 45, 42, 43], cnn-based [31], and graph-based models [53, 58]. These architectures aim to address the challenges posed by the irregularity and unordered nature of point clouds and enable effective point cloud analysis.

One of the main challenges in point cloud analysis is efficiently exploring local and global features while considering the irregular and disordered characteristics of point clouds. Recently, transformer architectures, which enable effective local/global-range learning via the attention mechanism, have become popular in both natural language processing [5, 12, 55] and computer vision [13, 34, 56, 57]. Inspired by this, transformer architectures have been further introduced for point cloud analysis [19, 25, 40, 75]. However, the vanilla self-attention module in transformer has a time complexity of $\mathcal{O}(N^2)$ when operating on a sequence of tokens with length N . When taking each point as a token, the $\mathcal{O}(N^2)$ complexity becomes unaffordable, as there are tens of thousands of points for each point cloud in real-world applications [3]. To address this challenge, [75] introduces vector self-attention in a local way, avoiding $\mathcal{O}(N^2)$ complexity by only interacting features with K neighbors (*e.g.*,

$K = 16$), while failing to capture long-range contexts. On the other hand, [25] employs local window-based self-attention with a shifted window strategy similar to [34] and proposes to capture long-range contexts by sampling nearby points densely and distant points sparsely. Nevertheless, due to the heterogeneous density distribution of point clouds, the fixed-size window partition employed in [25] leads to a diverse number of points in each local window, thus requiring complicated and sophisticated designs during implementation.

In this paper, we propose a new collect-and-distribute transformer, CDFormer, to learn both short- and long-range contexts for 3D point cloud analysis. Specifically, we first divide the point cloud into a set of local patches using K nearest neighbor points, instead of a fixed window partition [25]. Each local patch contains the same number of points, enabling direct modeling by popular deep learning packages [1, 41] without custom operations and avoids the prohibitive $\mathcal{O}(N^2)$ time complexity. Besides local self-attention for short-range interactions within each local patch, we introduce a collect-and-distribute mechanism. This mechanism first collects local patch information to a set of proxy reference points, explores long-range contexts among these reference points, and distributes the collected long-range contexts back to local points through cross-attention between reference points and local points. An illustration of the proposed collect-and-distribute mechanism is shown in Figure 1. To enhance local-global structure learning, the positional information is critical for transformers employed in point clouds [25, 75]. Therefore, we introduce context-aware position encoding for CDFormer, where the relative position information interacts with the input features to dynamically enhance the positional clues.

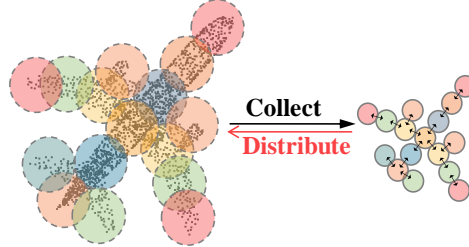


Figure 1: An illustration of the proposed collect-and-distribute mechanism.

Our main contributions can be summarized as follows:

- We propose CDFormer to capture short- and long-range contexts simultaneously with a novel collect-and-distribute mechanism, effectively learning local-global structures.
- We introduce context-aware position encoding to enhance position clues and facilitate communications within points.
- We conduct comprehensive experiments on four widely-used point cloud datasets, including ModelNet40 [61] and ScanObjectNN [54] for classification, and S3DIS [3] and ShapeNet-Part [69] for segmentation. Our experiments demonstrate the effectiveness of CDFormer and achieve state-of-the-art performances in point cloud analysis.

2 Related Work

Transformer Architectures. Transformer architectures have emerged as a dominant framework for natural language processing in recent years [12, 55]. In addition, they have seen widespread exploration in the realm of vision tasks, with ViT [13] being a groundbreaking work that divides images into local patches and treats each patch as a token. Building upon the success of ViT, numerous subsequent works have been proposed that either explore hierarchical architectures with multi-scale resolutions [15, 18, 30, 34, 56, 57] or incorporate local-global information [10, 28, 67]. For instance, PVT [56] devises a progressive shrinking pyramid to effectively explore multi-resolution features while HRViT [18] integrates high-resolution multi-branch architectures to learn multiplicative scale representations. Twins-SVT [10] incorporates locally-grouped self-attention and global sub-sampled attention to capture local-global contexts. Swin Transformer [34] introduces a hierarchical transformer architecture equipped with the shifted window strategy to enable cross-window communications. SepViT [28] proposes a self-attention mechanism that is depthwise separable to facilitate efficient local and global information exchange within a single attention block.

Point Cloud Analysis. The mainstream point cloud analysis methods can be roughly divided into three groups: point-based [19, 25, 31, 37, 40, 45, 42, 43, 53, 58, 63, 75], voxel-based [7, 50, 76], and projection-based [11, 38, 72]. For a better trade-off between complexity and efficiency, we

focus primarily on point-based approaches, where existing methods usually devise novel operations/architectures for raw points, including mlp-based [37, 45, 42, 43], cnn-based [31], graph-based [53, 58], and transformer-based [19, 25, 40, 75]. A pioneering work in this field is PointNet [42], which directly processes point clouds using multi-layer perceptrons (MLPs). This approach was further improved upon by PointNet++ [43], which introduced a hierarchical structure for processing point clouds. PointNext [45] proposes even more improved training strategies that significantly improve upon PointNet++ [43]. PointCNN [31] learns an x-transformation from the input points for alignment, which is followed by typical convolution layers. In contrast, KPConv [53] introduces kernel point convolution, a new point convolution operator, that takes neighboring points as input and processes them with spatially located weights. Recently, transformer architectures have been introduced for point cloud analysis [19, 25, 40, 75]. PCT [19] presents the offset-attention mechanism, which replaces the original self-attention. Point Transformer [75] introduces a vector self-attention mechanism to aggregate neighbor features but fails to capture long-range dependencies. Stratified Transformer [25] captures long-range contexts by sampling nearby points densely and distant points sparsely with the shifted window strategy, as used in Swin Transformer [34]. However, due to the varying density distribution of point clouds, partitioning windows in a fixed size may lead to varying point counts in different local windows, necessitating complex and sophisticated designs to address this issue.

3 Method

In this section, we first provide an overview of the proposed CDFormer for 3D point cloud analysis. We then introduce the patch division and the collect-and-distribute mechanism in detail. Lastly, we discuss the proposed context-aware position encoding.

3.1 Overview

A 3D point cloud usually consists of a set of N points $\mathbf{P} \in \mathbb{R}^{N \times 3}$, where each point is featured by the Cartesian coordinate (x, y, z) . The objective of typical point cloud analysis tasks is to assign semantic labels to the point cloud. For example, for point cloud classification, the goal is to predict a single semantic label $Q \in \{0, \dots, U-1\}$ for the whole point cloud \mathbf{P} , where U is the total number of semantic categories; For point cloud segmentation, the goal is to assign a semantic label for each point in the point cloud \mathbf{P} .

The main CDFormer framework for 3D point cloud analysis is illustrated by Figure 2. Since a point cloud may also contain extra features such as color, we consider the input feature of a general point cloud as $\mathbf{X} \in \mathbb{R}^{N \times C}$, where C indicates the number of feature channels. Specifically, we first utilize a KPConv [53] layer as the embedding layer to aggregate local information for raw point embeddings to obtain the embedded features with the size of $N \times C_1$. After that, the main backbone network is a stack of multiple the proposed collect-and-distribute blocks or CD Blocks, where each block first divides all points into local patches and then explores short- and long-range contexts in a collect-and-distribute manner as follows: 1) a local self-attention is first used to learn short-range relations in each patch of points; 2) the learned local features are then collected to a set of proxy reference points which then communicate with each other to capture long-range contexts; and 3) the learned long-range contexts are finally distributed back to the original local patch points such that the learned point embeddings are equipped with both short- and long-range information.

3.2 Patch Division

For a typical point cloud with tens of thousands of points [3], it is computationally prohibitive to consider each point as a token: given a sequence of tokens with the length N , the time complexity of the self-attention in transformer is $\mathcal{O}(N^2)$. Therefore, following [13, 39, 70], we divide a point cloud into multiple local patches, *e.g.*, M patches with K points in each patch, and then employ self-attention within each local patch instead of all points. Therefore, with a proper patch division, it becomes acceptable with a linear time complexity $\mathcal{O}(MK^2)$.

We describe the patch division process used in our method as follows. Given a scale factor S , the point cloud $\mathbf{X} \in \mathbb{R}^{N \times C}$ is divided into $M = N/S$ patches, and The furthest point sampling algorithm (FPS) [14, 43] is utilized on the point features $\mathbf{X} \in \mathbb{R}^{N \times C}$ to obtain patch centers

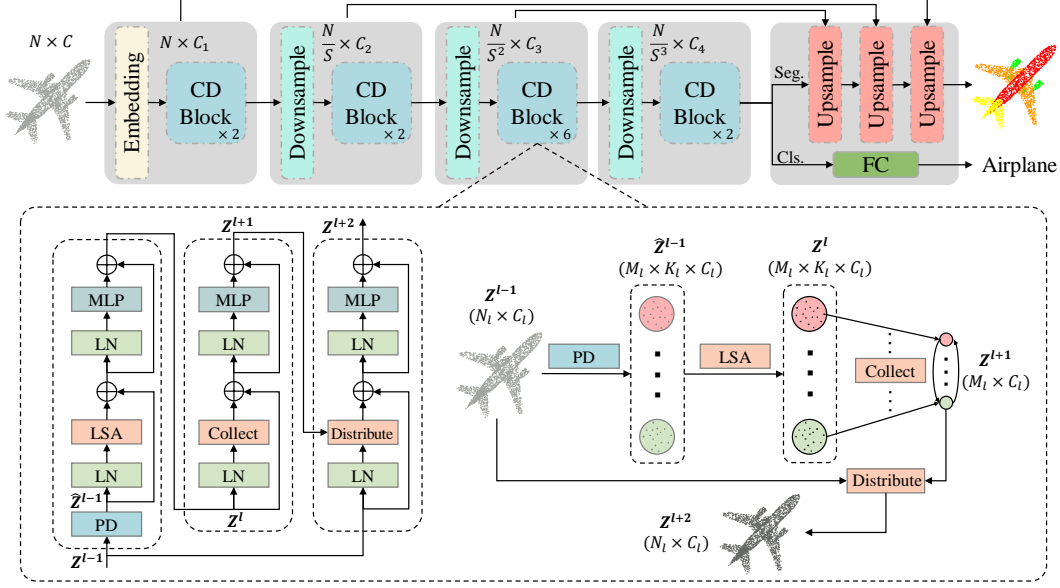


Figure 2: The main collect-and-distribute transformer framework. Note that **PD** refers to patch division and **LSA** indicates the local self-attention defined by Eq. (1).

$\bar{\mathbf{X}} \in \mathbb{R}^{M \times C}$. For each local patch, we group the K nearest neighbors around each patch center and reformulate M patches as $\hat{\mathbf{X}} \in \mathbb{R}^{M \times K \times C}$, and then apply the local self-attention (LSA) to extract local features. Specifically, for the i_{th} patch where $i \in [0, \dots, M-1]$, let $\hat{\mathbf{x}} \in \mathbb{R}^{K \times C}$ denote its representation, which is then fed into MLPs to generate the query token $\mathbf{Q}_{lsa} = \mathbf{W}_{lsa}^q \hat{\mathbf{x}}$, the key token $\mathbf{K}_{lsa} = \mathbf{W}_{lsa}^k \hat{\mathbf{x}}$, and the value token $\mathbf{V}_{lsa} = \mathbf{W}_{lsa}^v \hat{\mathbf{x}}$, respectively. The output $\bar{\mathbf{z}} \in \mathbb{R}^{K \times C}$ can thus be calculated as follows:

$$\bar{\mathbf{z}} = \mathbf{W}_{lsa}^{attn} \mathbf{V}_{lsa}, \quad \mathbf{W}_{lsa}^{attn} = \text{softmax}((\mathbf{Q}_{lsa} \mathbf{K}_{lsa}^\top) / \sqrt{C}), \quad (1)$$

where all M patches features can be similarly obtained as $\bar{\mathbf{Z}} \in \mathbb{R}^{M \times K \times C}$. Notably, we don't discuss the position encoding here and leave it in Sec 3.4. Lastly, we have the complexity as follows: the local self-attention in each patch only has the time complexity $\mathcal{O}(K^2)$, and the overall time complexity of M patches become affordable $\mathcal{O}(MK^2) = \mathcal{O}(NK^2/S)$. Through LSA, all points in each local patch can communicate with each other to capture short-range dependencies.

3.3 Collect-and-Distribute Mechanism

As the aforementioned local self attention only models the short-range information in each local patch, we then introduce how to explore long-range contexts with the proposed collect-and-distribute mechanism. Specifically, we first collect those communicated local feature as a set of proxy reference points such that each local patch directly corresponds to a specific proxy point. To capture the long-range dependencies, a neighbor self-attention (NSA) is then applied on those proxy references to allow feature propagation among neighbors. By doing this, we can extract long-range contexts with a reduced linear time complexity since each proxy represents a patch of points. Lastly, those enhanced proxies distribute back to the local points via cross-attention to achieve short- and long-range contexts communications. An illustration of the proposed block is shown in Figure 3, and we depict each step in detail as follows.

Collect. Given local patches $\bar{\mathbf{Z}} \in \mathbb{R}^{M \times K \times C}$, we collect local patch information from K local points to a proxy reference point via a max-pooling operation, $\mathbf{R} = \text{maxpool}(\bar{\mathbf{Z}}) \in \mathbb{R}^{M \times C}$. Next, we consider the K nearest neighbors for each proxy $\hat{\mathbf{R}} \in \mathbb{R}^{M \times K \times C}$ to capture the long-range contexts by employing a neighboring self-attention between \mathbf{R} and $\hat{\mathbf{R}}$, *i.e.*, a self-attention between each proxy and its K neighbors followed by a sum operation to generate the output $\hat{\mathbf{Z}} \in \mathbb{R}^{M \times C}$. We first generate the feature embeddings with MLPs for query, key, and value by $\mathbf{Q}_{nsa} = \mathbf{W}_{nsa}^q \mathbf{R}$,

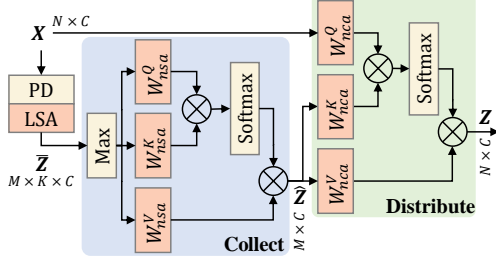


Figure 3: An illustration of the proposed CD Block.

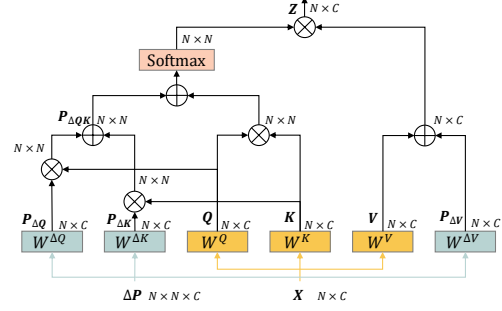


Figure 4: An illustration of context-aware position encoding.

$\mathbf{K}_{nsa} = \mathbf{W}_{nsa}^k \hat{\mathbf{R}}$, and $\mathbf{V}_{nsa} = \mathbf{W}_{nsa}^v \hat{\mathbf{R}}$, respectively. Then we can formulate as follows:

$$\hat{\mathbf{Z}} = \text{Sum}(\mathbf{W}_{nsa}^{attn} \mathbf{V}_{nsa}), \quad \mathbf{W}_{nsa}^{attn} = \text{Softmax}((\mathbf{Q}_{nsa} \mathbf{K}_{nsa}^\top) / \sqrt{C}). \quad (2)$$

Notably, the time complexity $\mathcal{O}(NK^2/S)$ is linear to N because the NSA is only applied on K neighbors instead of all proxies.

Distribute. We distribute the long-range information in $\hat{\mathbf{Z}} \in \mathbb{R}^{M \times C}$ back to local patch points for joint short- and long-range contexts via a neighboring cross-attention (NCA). In particular, given vanilla point features $\mathbf{X} \in \mathbb{R}^{N \times C}$ and enhanced proxies $\hat{\mathbf{Z}} \in \mathbb{R}^{M \times C}$, we first group the K nearest neighbor proxies $\mathbf{E} \in \mathbb{R}^{M \times K \times C}$ for each point. After that, we employ the neighbor cross-attention by regarding \mathbf{X} as the query, \mathbf{E} as the key and value, which is fed into a successive sum operation to obtain the final output $\mathbf{Z} \in \mathbb{R}^{N \times C}$. We first get the embeddings with MLPs by $\mathbf{Q}_{nca} = \mathbf{W}_{nca}^q \mathbf{X}$, $\mathbf{K}_{nca} = \mathbf{W}_{nca}^k \mathbf{E}$, and $\mathbf{V}_{nca} = \mathbf{W}_{nca}^v \mathbf{E}$, respectively. After that, we can calculate \mathbf{Z} as follows:

$$\mathbf{Z} = \text{Sum}(\mathbf{W}_{nca}^{attn} \mathbf{V}_{nca}), \quad \mathbf{W}_{nca}^{attn} = \text{Softmax}((\mathbf{Q}_{nca} \mathbf{K}_{nca}^\top) / \sqrt{C}). \quad (3)$$

In this way, each point communicates with K enhanced proxies, *i.e.*, $K \times K$ original proxies, and $K \times K \times K$ original points. Therefore, the long-range dependencies can be effectively distributed back to local points, *i.e.*, both short- and long-range contexts are fused into the learned representations.

3.4 Context-Aware Position Encoding

The position information of input tokens is necessary for transformer architectures [13, 55], while 3D point cloud naturally contains the (x, y, z) coordinates as position. Therefore, it might be straightforward to remove position encoding in the transformer-based architecture for point clouds. However, when the network goes deeper, the coordinates information can not keep precisely intact [25, 75]. Inspired by [59], we propose to further enhance the position clues in point cloud transformer via a context-aware position encoding (CAPE). Specifically, CAPE is calculated by interacting relative position differences with the current features, thus can simultaneously handle the unordered characteristic of the point cloud and adaptively enhance the position information. An illustration of the proposed context-aware position encoding is shown in Figure 4.

Given the input $\mathbf{X} \in \mathbb{R}^{N \times C}$ and the relative position differences $\Delta \mathbf{P} \in \mathbb{R}^{N \times N \times 3}$, we first obtain the $\mathbf{Q}, \mathbf{K}, \mathbf{V}$ and their position embeddings $\mathbf{P}_{\Delta q}, \mathbf{P}_{\Delta k}, \mathbf{P}_{\Delta v}$ via MLPs. We then calculate the CAPE $\mathbf{P}_{\Delta qk} = \mathbf{P}_{\Delta q} \mathbf{Q}^\top + \mathbf{P}_{\Delta k} \mathbf{K}^\top$ such that it is aware of the input features and can dynamically magnify the position information to effectively facilitate the communication of points. Lastly, we obtain the output $\mathbf{Z} \in \mathbb{R}^{N \times C}$ as follows:

$$\mathbf{Z} = \mathbf{W}_{attn} \cdot (\mathbf{V} + \mathbf{P}_{\Delta v}), \quad \mathbf{W}_{attn} = \text{Softmax}((\mathbf{Q} \mathbf{K}^\top + \mathbf{P}_{\Delta qk}) / \sqrt{C}). \quad (4)$$

Notably, if not otherwise stated, we use CAPE in all attention layers, including LSA, NSA, and NCA, to better capture short- and long-range contexts.

4 Experiments

In this section, we first introduce the implementation details. We then evaluate the proposed CDFormer on ModelNet40 [61] and ScanObjectNN [54] for point cloud classification, ShapeNetPart [69] for

Table 1: Results on ModelNet40.

Method	Inputs	#Points	OA(%)
PointNet [42]	xyz	1024	89.2
PointNet++ [43]	xyz	1024	90.7
PointNet++ [43]	xyz+norm	5000	91.9
PointCNN [31]	xyz	1024	92.5
PointConv [60]	xyz+norm	1024	92.5
A-CNN [24]	xyz+norm	1024	92.6
KPConv [53]	xyz	7000	92.9
DGCNN [58]	xyz	1024	92.9
PointASNL [66]	xyz	1024	92.9
PointNext [45]	xyz	1024	93.2
PosPool [33]	xyz	5000	93.2
PCT [19]	xyz	1024	93.2
SO-Net [27]	xyz	5000	93.4
Point Trans. [75]	xyz	1024	93.7
PA-DGC [64]	xyz	1024	93.9
PointMLP [37]	xyz	1024	94.1
CDFormer (ours)	xyz	1024	<u>94.0</u>

Table 2: Results on ScanObjectNN.

Method	mAcc(%)	OA(%)
PointNet [42]	63.4	68.2
SpiderCNN [65]	69.8	73.7
PointNet++ [43]	75.4	77.9
DGCNN [58]	73.6	78.1
PointCNN [31]	75.1	78.5
BGA-DGCNN [54]	75.7	79.7
BGA-PN++ [54]	77.5	80.2
DRNet [46]	78.0	80.3
GBNet [47]	77.8	80.5
SimpleView [17]	-	80.5±0.3
PRANet [8]	79.1	82.1
MVTN [20]	-	82.8
PointMLP [37]	83.9±0.5	85.4±0.3
PointNext [45]	85.8±0.6	87.7±0.4
CDFormer (ours)	87.2±0.3	88.4±0.2

point cloud part segmentation, and S3DIS [3] for point cloud scene segmentation. Lastly, we perform comprehensive ablation studies on each component.

4.1 Implementation Details.

For ModelNet40 [61], following [45], we use fewer blocks in each stage $[1, 1, 3, 1]$ with larger feature dimensions $\mathcal{C} = [64, 128, 256, 512]$ and larger number of heads $\mathcal{H} = [4, 8, 16, 32]$. We simply use $K = 16$ neighbours in all blocks. Cosine annealing schedule with learning rate 0.001 is adopted for training 600 epochs with batch size 32. We use AdamW optimizer [35] with the weight decay 0.05. For each data sample, only 1,024 points with (x, y, z) are used for training and testing, and common data augmentations, including shift, scale and cutmix [71], are employed. The downsampling scale S of each stage is set to 4. For ScanObjectNN [54], we follow [45] to use point resampling to adapt 1,024 points for training, and only the hardest perturbed variant (PB_T50_RS) is considered in our experiment. We keep other training configurations the same as those in ModelNet40.

For S3DIS [3], following the practice in [25, 75], we first apply the grid sampling on the raw input points with the grid size 0.04m. We adopt the encoder with four stages with $[2, 2, 6, 2]$ blocks, the number of channels $\mathcal{C} = [C_1, C_2, C_3, C_4] = [48, 96, 192, 384]$ and the number of heads $\mathcal{H} = [H_1, H_2, H_3, H_4] = [3, 6, 12, 24]$. For simplicity, we set neighbours $K = 16$ in all blocks. During the training process, the maximum number of input points is set to 80,000. Meanwhile, we set the downsampling scale S of each stage to 8. We use AdamW optimizer [35] with the weight decay 0.01. All models are trained for 100 epochs, and the learning rate starts from 0.01 and drops by 1/10 at 60 and 80 epochs. We use four V100 GPUs with the batch size of 8. Following [45], we use the cross-entropy loss with label smoothing, and popular data augmentations including jitter, scale, rotate, and color drop. For ShapeNetPart [69], we follow [45] to use 2,048 points for training and testing. Considering that each point cloud has fewer points than it in S3DIS [3], we reduce the downsampling scale S to 4 and use the batch size 80. The model is trained for 300 epochs, and the learning rate starts from 0.01 and drops by 1/10 at 210 and 270 epochs. Other settings are same as those in S3DIS.

4.2 Point Cloud Classification

Dataset and Metrics. ModelNet40 [61] is a canonical dataset for object shape classification, which consists of 9,843 training and 2,468 testing CAD models belonging to 40 categories. We report the results of overall accuracy (OA). ScanObjectNN [54] is a more challenging real-world benchmark in terms of background, noise, and occlusions. It contains totally 15,000 objects from 15 classes. We report the results of the mean of class-wise accuracy (mAcc) and overall accuracy (OA) on hardest perturbed variant (PB_T50_RS).

Table 3: Results on ShapeNetPart [69].

Method	Ins. mIoU	Throughput
PointNet [42]	83.7	1184
PointNet++ [43]	85.1	708
DGCNN [58]	85.2	147
ASSANet-L [44]	86.1	640
PointMLP [37]	86.1	270
KPConv [53]	86.4	44
Point Transformer [75]	86.6	297
Stratified Transformer [25]	86.6	398
CurveNet [62]	<u>86.8</u>	97
PointNeXt [45]	87.0	76
CDFormer (ours)	87.0	84

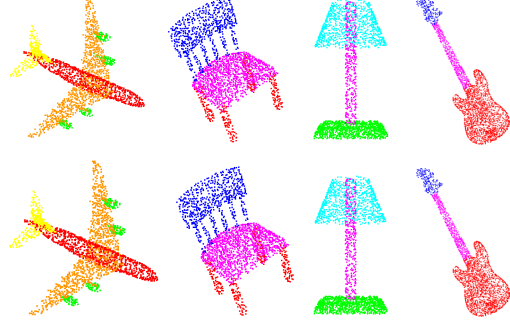


Figure 5: Visualizations of part segmentation from ground truth (top) and CDFormer (bottom).

Results. Table 1 shows the results on ModelNet40, where the proposed CDFormer achieves comparable performance 94.0% with other state-of-the-arts by only taking 1,024 points as input. In Table 2, we also evaluate the proposed method on the most challenging variant (PB_T50_RS) of ScanObjectNN, where CDFormer achieves 87.2 ± 0.3 and 88.4 ± 0.2 on mAcc and OA, significantly outperforming all previous methods in terms of both performance and stability. Specifically, PointMLP [37] obtains 94.1% on ModelNet40, but we surpass it by over 3% in ScanObjectNN and also show more stable performance as indicated by the smaller standard derivation. PointNeXt [45] is the current state-of-the-art method, but we still outperform it by a clear margin, especially on mAcc (87.2% vs. 85.8%). Also, the smallest gap between mean of class-wise accuracy (mAcc) and overall accuracy (OA) achieved by CDFormer implies that our approach shows excellent robust performance on each class instead of biasing to a specific category. We owe it to the proposed collect-and-distribute mechanism for effectively capturing both short- and long-range contexts, which can handle different categories with different scales and shapes.

4.3 Point Cloud Part Segmentation

Dataset and Metrics. ShapeNetPart [69] is a popular dataset for object part segmentation, which is composed of 16,880 3D models from 16 different shape categories (*e.g.*, *airplane* and *chair*), where 14,006 models for training and 2,874 for testing. For each category, its number of parts is between 2 and 6, and there are total 50 different parts. For evaluation metrics, we report the instance mIoU along with the throughput speed (*instance/second*).

Results. Table 3 demonstrates the results of CDFormer compared to previous approaches. Our CDFormer outperforms congeneric transformer-based methods, *e.g.*, Point Transformer [75] and Stratified Transformer [25], and other representative approaches like KPConv [53], while it is comparable to the best results of PointNext [45] (87.0% vs. 87.0%). As we will see from Table 4 that the CDFormer defeats PointNext on S3DIS (76.0% vs. 74.9%), we thus conjecture that the collect-and-distribute mechanism in CDFormer can not fully exploit the advantage of capturing long-range dependencies on the small size of point cloud considering the huge difference on the size of samples in ShapeNetPart (2,048) and S3DIS (up to 80,000 during training). The part segmentation results of multiple objects are visualized in Figure 5. As observed, the predictions from CDFormer are semantically reasonable and close to the ground truth.

4.4 Point Cloud Scene Segmentation

Dataset and Metrics. S3DIS [3] is a challenging benchmark for point cloud scene segmentation, containing 271 rooms in 6 areas collected from three buildings. The point is annotated with 13 semantic categories such as *ceiling* and *bookcase*. Following [43, 75], we evaluate the proposed method on Area 5 and also perform standard 6-fold cross-validation. We report performances using mean class-wise intersection over union (mIoU), mean of class-wise accuracy (mAcc), and overall point-wise accuracy (OA).

Results. In Table 4, the proposed CDFormer achieves new state-of-the-art performances on both Area 5 and standard 6-fold cross-validation. Notably, the recent method PointNext [45] has 41.6M param-

Table 4: Results on S3DIS [3]. The **bold** and underline denote the first and second best performances.

Method	S3DIS 6-Fold			S3DIS Area 5		
	mIoU (%)	mACC (%)	OA (%)	mIoU (%)	mACC (%)	OA (%)
PointNet [42]	47.6	66.2	78.6	41.1	49.0	-
RSNet [22]	56.5	66.5	-	51.9	59.4	-
SPG [26]	62.1	73.0	85.5	58.0	66.5	86.4
PointCNN [31]	65.4	75.6	88.1	57.3	63.9	85.9
PointWeb [74]	66.7	76.2	87.3	60.3	66.6	87.0
ShellNet [73]	66.8	-	87.1	-	-	-
RandLA-Net [21]	70.0	82.0	88.0	-	-	-
KPCConv [53]	70.6	79.1	-	67.1	72.8	-
SCF-Net [16]	71.6	82.7	88.4	63.4	-	-
BAAF [48]	72.2	<u>83.1</u>	88.9	65.4	-	-
CBL [51]	73.1	79.4	89.6	69.4	75.2	90.6
Point Transformer [75]	73.5	81.9	90.2	70.4	76.5	90.8
Stratified Transformer [25]	-	-	-	<u>72.0</u>	<u>78.1</u>	91.5
DeepViewAgg [49]	74.7	-	-	67.2	-	-
PointNext [45]	<u>74.9</u>	83.0	<u>90.3</u>	70.5	76.8	90.6
CDFormer (ours)	76.0	84.6	90.7	72.2	78.5	<u>91.2</u>

ters for its best results, while our CDFormer with 25.7M parameters achieves a clear improvement of 1.7% and 1.1% mIoU under Area 5 and 6-fold cross-validation. Additionally, with and without using 2D images, DeepViewAgg [49] obtains 69.5% and 74.7% respectively, which nevertheless is also inferior to the proposed method (76.0%). Additionally, we provide some visualizations in Figure 6.

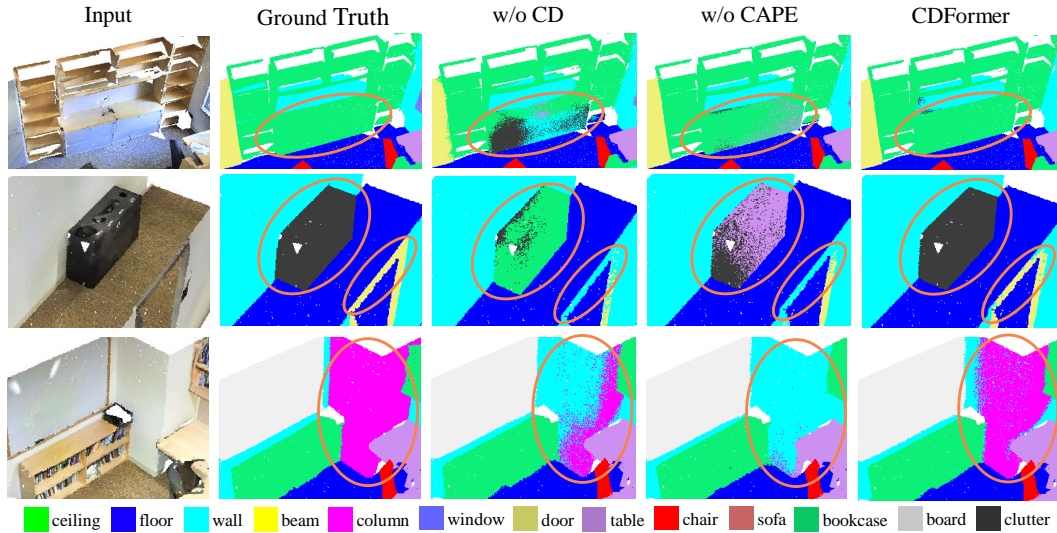


Figure 6: Visualization of scene segmentation on S3DIS. The improved areas against baselines are highlighted by the orange circles.

4.5 Ablation Studies

In this subsection, we conduct ablation studies on Area 5 of S3DIS.

Collect-and-Distribute Mechanism. To explore the effectiveness of the proposed collect-and-distribute mechanism, we use the counterpart vanilla parameter-free (or tiny) operations as baselines. Specifically, we only keep the max operation to aggregate local features while discarding neighbor self-attention when no *collect*. Also, we adopt an interpolation layer followed by a simple MLP to add back to local points if no *distribute*. In Table 5, we find that without the collect-and-distribute mechanism, it achieves a relatively low mIoU 67.6%, which is then improved by *collect* for catching the long-range dependencies to 70.1%. Furthermore, when further distributing the long-range contexts back to the local points, we achieve the best performances on all metrics, *i.e.*, 72.2% mIoU, 78.5% mAcc, and 91.2% OA. Besides, if without *collect* to explicitly and broadly explore long-range dependencies, using the max aggregation with *Distribute* (ses iii) significantly drops the performance from 72.2% to 70.3% on mIoU.

Table 5: Ablation study on the collect-and-distribute mechanism.

cfg	LSA	Collect	Distribute	mIoU	mAcc	OA
i	✓			67.6	74.1	89.7
ii	✓	✓		70.1	76.6	90.7
iii	✓		✓	70.3	77.0	90.7
iv	✓	✓	✓	72.2	78.5	91.2

Table 6: Ablation study on the context-aware position encoding.

cfg	QKV	CA	Plain	mIoU	mAcc	OA
i				68.9	76.6	89.7
ii	✓			69.7	76.3	91.0
iii	✓	✓		72.2	78.5	91.2
iv	✓		✓	70.8	77.5	90.9

Context-Aware Position Encoding. To evaluate the influence of position encoding, we compare the proposed method with and without using the position encoding in the query, key, and value (**QKV**), respectively. We also compare the context-aware (**CA**) format of position encoding with a vanilla one (*i.e.*, **Plain**) as in [13]. As shown in Table 6, without the position encoding, we have dissatisfied results that are consistent with the observations in [25, 75]. Next, we employ a normal encoding without context-aware format (see ii) on QKV, *i.e.*, no interaction with the contexts Q, K. This time, it does work but with only marginal improvement. Lastly, when using the proposed CAPE (see iii), it can achieve the state-of-the-art performance 72.2%. Through the dynamic adaptation based on input contexts, the position clues are further enhanced in the proposed CDFormer to effectively learn local-global relations. Additionally, we also show the results of using a vanilla version of position encoding [13] (see iv) for a fair comparison.

Model Scalability. We evaluate the model scalability under four stages with [2, 2, 6, 2] blocks via the following three configurations:

- CDFormer-S: $\mathcal{C} = [16, 32, 64, 128]$, $\mathcal{H} = [1, 2, 4, 8]$
- CDFormer-B: $\mathcal{C} = [32, 64, 128, 256]$, $\mathcal{H} = [2, 4, 8, 16]$
- CDFormer-L: $\mathcal{C} = [48, 96, 192, 384]$, $\mathcal{H} = [3, 6, 12, 24]$

As shown in Table 7, there are clear performance improvements when using a larger model. For example, the improvements are very impressive in terms of both mIoU and mAcc, *i.e.*, mIoU: 67.6% \rightarrow 69.7% \rightarrow 72.2%; mAcc: 74.9% \rightarrow 77.1% \rightarrow 78.5%. Notably, the consistent improvements by increasing the model size illustrate the extraordinary scalability of the proposed CDFormer for point cloud analysis.

Table 7: Ablation study on model scalability.

Model	#Params	mIoU	mAcc	OA
CDFormer-S	3.1M	67.6	74.9	89.8
CDFormer-B	11.7M	69.7	77.1	90.4
CDFormer-L	25.7M	72.2	78.5	91.2

Table 8: Ablation study on number of neighbors.

cfg	K	mIoU	mAcc	OA
i	4	69.2	75.7	90.3
ii	8	71.1	77.9	91.4
iii	16	72.2	78.5	91.2

Number of Neighbors. We show the influences for using the different number of neighbors in CD Blocks for patch division, NSA, and NCA. For simplicity, we use the same K for all modules and stages. As show in Table 8, when increasing the number of neighbors from $K = 4$ to $K = 8$, the improvement (69.2% \rightarrow 71.1%) is significant. This is possibly because a relatively large number of neighbors can bring better long-range contexts, which help the proposed CDFormer learn the local-global structures. Notably, we also find that the advancement from $K = 8$ to $K = 16$ is modest. This kind of saturated phenomenon is expected since too much contexts may introduce different categories of semantics that degrade the local features. Similar observations have also been reported in [75]. Therefore, we use $K = 16$ as default.

5 Conclusion

In this paper, we propose the novel CDFormer for 3D point cloud analysis. Using the proposed collect-and-distribute mechanism, it can capture short- and long-range contexts simultaneously to effectively learn local-global point cloud representation. Additionally, we introduce context-aware position encoding to dynamically enhance position clues further and facilitate capturing short- and long-range contexts. Comprehensive experiments conducted on S3DIS, ShapeNetPart, ModelNet40 and ScanObjectNN for segmentation and classification demonstrate the superiority of CDFormer and the benefits of each design.

References

- [1] Martin Abadi, Paul Barham, Jianmin Chen, Zhifeng Chen, Andy Davis, Jeffrey Dean, Matthieu Devin, Sanjay Ghemawat, Geoffrey Irving, Michael Isard, Manjunath Kudlur, Josh Levenberg, Rajat Monga, Sherry Moore, Derek G. Murray, Benoit Steiner, Paul Tucker, Vijay Vasudevan, Pete Warden, Martin Wicke, Yuan Yu, and Xiaoqiang Zheng. Tensorflow: A system for large-scale machine learning. In *12th USENIX Symposium on Operating Systems Design and Implementation (OSDI 16)*, pages 265–283, 2016. [1](#), [15](#)
- [2] Eren Erdal Aksoy, Saimir Baci, and Selcuk Cavdar. Salsanet: Fast road and vehicle segmentation in lidar point clouds for autonomous driving. In *IEEE Intelligent Vehicles Symposium*, pages 926–932, 2020. [1](#)
- [3] Iro Armeni, Ozan Sener, Amir R Zamir, Helen Jiang, Ioannis Brilakis, Martin Fischer, and Silvio Savarese. 3d semantic parsing of large-scale indoor spaces. In *IEEE/CVF Conference on Computer Vision and Pattern Recognition (CVPR)*, pages 1534–1543, 2016. [1](#), [2](#), [3](#), [6](#), [7](#), [8](#), [14](#), [15](#)
- [4] J. Behley, M. Garbade, A. Milioto, J. Quenzel, S. Behnke, C. Stachniss, and J. Gall. SemanticKITTI: A Dataset for Semantic Scene Understanding of LiDAR Sequences. In *IEEE/CVF International Conference on Computer Vision (ICCV)*, 2019. [16](#)
- [5] Tom Brown, Benjamin Mann, Nick Ryder, Melanie Subbiah, Jared D Kaplan, Prafulla Dhariwal, Arvind Neelakantan, Pranav Shyam, Girish Sastry, Amanda Askell, et al. Language models are few-shot learners. *Advances in Neural Information Processing Systems (NeurIPS)*, 33:1877–1901, 2020. [1](#)
- [6] Holger Caesar, Varun Bankiti, Alex H Lang, Sourabh Vora, Venice Erin Liong, Qiang Xu, Anush Krishnan, Yu Pan, Giancarlo Baldan, and Oscar Beijbom. nuscenes: A multimodal dataset for autonomous driving. In *IEEE/CVF Conference on Computer Vision and Pattern Recognition (CVPR)*, pages 11621–11631, 2020. [16](#)
- [7] Ran Cheng, Ryan Razani, Ehsan Taghavi, Enxu Li, and Bingbing Liu. 2-s3net: Attentive feature fusion with adaptive feature selection for sparse semantic segmentation network. In *IEEE/CVF Conference on Computer Vision and Pattern Recognition (CVPR)*, pages 12547–12556, 2021. [2](#)
- [8] Silin Cheng, Xiwu Chen, Xinwei He, Zhe Liu, and Xiang Bai. Pra-net: Point relation-aware network for 3d point cloud analysis. *IEEE Transactions on Image Processing (TIP)*, 30:4436–4448, 2021. [6](#)
- [9] Christopher Choy, JunYoung Gwak, and Silvio Savarese. 4d spatio-temporal convnets: Minkowski convolutional neural networks. In *IEEE/CVF Conference on Computer Vision and Pattern Recognition (CVPR)*, pages 3075–3084, 2019. [14](#)
- [10] Xiangxiang Chu, Zhi Tian, Yuqing Wang, Bo Zhang, Haibing Ren, Xiaolin Wei, Huaxia Xia, and Chunhua Shen. Twins: Revisiting the design of spatial attention in vision transformers. *Advances in Neural Information Processing Systems (NeurIPS)*, 34, 2021. [2](#)
- [11] Tiago Cortinhal, George Tzelepis, and Eren Erdal Aksoy. Salsanext: Fast, uncertainty-aware semantic segmentation of lidar point clouds. In *International Symposium on Visual Computing (ISVC)*, pages 207–222, 2020. [2](#)
- [12] Jacob Devlin, Ming-Wei Chang, Kenton Lee, and Kristina Toutanova. Bert: Pre-training of deep bidirectional transformers for language understanding. *arXiv preprint arXiv:1810.04805*, 2018. [1](#), [2](#)
- [13] Alexey Dosovitskiy, Lucas Beyer, Alexander Kolesnikov, Dirk Weissenborn, Xiaohua Zhai, Thomas Unterthiner, Mostafa Dehghani, Matthias Minderer, Georg Heigold, Sylvain Gelly, et al. An image is worth 16x16 words: Transformers for image recognition at scale. *arXiv preprint arXiv:2010.11929*, 2020. [1](#), [2](#), [3](#), [5](#), [9](#)
- [14] Yuval Eldar, Michael Lindenbaum, Moshe Porat, and Yehoshua Y Zeevi. The farthest point strategy for progressive image sampling. *IEEE Transactions on Image Processing (TIP)*, 6(9):1305–1315, 1997. [3](#)
- [15] Haoqi Fan, Bo Xiong, Karttikeya Mangalam, Yanghao Li, Zhicheng Yan, Jitendra Malik, and Christoph Feichtenhofer. Multiscale vision transformers. In *IEEE/CVF International Conference on Computer Vision (ICCV)*, pages 6824–6835, 2021. [2](#)
- [16] Siqi Fan, Qiulei Dong, Fenghua Zhu, Yisheng Lv, Peijun Ye, and Fei-Yue Wang. Scf-net: Learning spatial contextual features for large-scale point cloud segmentation. In *Proceedings of the IEEE/CVF Conference on Computer Vision and Pattern Recognition*, pages 14504–14513, 2021. [8](#), [15](#)

- [17] Ankit Goyal, Hei Law, Bowei Liu, Alejandro Newell, and Jia Deng. Revisiting point cloud shape classification with a simple and effective baseline. In *International Conference on Machine Learning (ICML)*, pages 3809–3820. PMLR, 2021. 6
- [18] Jiaqi Gu, Hyoukjun Kwon, Dilin Wang, Wei Ye, Meng Li, Yu-Hsin Chen, Liangzhen Lai, Vikas Chandra, and David Z Pan. Multi-scale high-resolution vision transformer for semantic segmentation. In *IEEE/CVF Conference on Computer Vision and Pattern Recognition (CVPR)*, pages 12094–12103, 2022. 2
- [19] Meng-Hao Guo, Jun-Xiong Cai, Zheng-Ning Liu, Tai-Jiang Mu, Ralph R Martin, and Shi-Min Hu. Pct: Point cloud transformer. *Computational Visual Media*, 7(2):187–199, 2021. 1, 2, 3, 6, 14
- [20] Abdullah Hamdi, Silvio Giancola, and Bernard Ghanem. Mvtn: Multi-view transformation network for 3d shape recognition. In *IEEE/CVF International Conference on Computer Vision (ICCV)*, pages 1–11, 2021. 6
- [21] Qingyong Hu, Bo Yang, Linhai Xie, Stefano Rosa, Yulan Guo, Zhihua Wang, Niki Trigoni, and Andrew Markham. Randla-net: Efficient semantic segmentation of large-scale point clouds. In *IEEE/CVF Conference on Computer Vision and Pattern Recognition (CVPR)*, pages 11108–11117, 2020. 8, 15
- [22] Qiangui Huang, Weiyue Wang, and Ulrich Neumann. Recurrent slice networks for 3d segmentation of point clouds. In *IEEE/CVF Conference on Computer Vision and Pattern Recognition (CVPR)*, pages 2626–2635, 2018. 8, 15
- [23] Li Jiang, Hengshuang Zhao, Shu Liu, Xiaoyong Shen, Chi-Wing Fu, and Jiaya Jia. Hierarchical point-edge interaction network for point cloud semantic segmentation. In *IEEE/CVF International Conference on Computer Vision (ICCV)*, pages 10433–10441, 2019. 14
- [24] Artem Komarichev, Zichun Zhong, and Jing Hua. A-cnn: Annularly convolutional neural networks on point clouds. In *IEEE/CVF Conference on Computer Vision and Pattern Recognition (CVPR)*, pages 7421–7430, 2019. 6
- [25] Xin Lai, Jianhui Liu, Li Jiang, Liwei Wang, Hengshuang Zhao, Shu Liu, Xiaojuan Qi, and Jiaya Jia. Stratified transformer for 3d point cloud segmentation. *IEEE/CVF Conference on Computer Vision and Pattern Recognition (CVPR)*, 2022. 1, 2, 3, 5, 6, 7, 8, 9, 14, 15
- [26] Loic Landrieu and Martin Simonovsky. Large-scale point cloud semantic segmentation with superpoint graphs. In *IEEE/CVF Conference on Computer Vision and Pattern Recognition (CVPR)*, pages 4558–4567, 2018. 8, 14, 15
- [27] Jiaxin Li, Ben M Chen, and Gim Hee Lee. So-net: Self-organizing network for point cloud analysis. In *IEEE/CVF Conference on Computer Vision and Pattern Recognition (CVPR)*, pages 9397–9406, 2018. 6
- [28] Wei Li, Xing Wang, Xin Xia, Jie Wu, Xuefeng Xiao, Min Zheng, and Shiping Wen. Sepvit: Separable vision transformer. *arXiv preprint arXiv:2203.15380*, 2022. 2
- [29] Xuyou Li, Shitong Du, Guangchun Li, and Haoyu Li. Integrate point-cloud segmentation with 3d lidar scan-matching for mobile robot localization and mapping. *Sensors*, 20(1):237, 2019. 1
- [30] Yanghao Li, Chao-Yuan Wu, Haoqi Fan, Karttikeya Mangalam, Bo Xiong, Jitendra Malik, and Christoph Feichtenhofer. Mvitv2: Improved multiscale vision transformers for classification and detection. In *IEEE/CVF Conference on Computer Vision and Pattern Recognition (CVPR)*, 2022. 2
- [31] Yangyan Li, Rui Bu, Mingchao Sun, Wei Wu, Xinhan Di, and Baoquan Chen. Pointcnn: Convolution on x-transformed points. *Advances in Neural Information Processing Systems (NeurIPS)*, 31, 2018. 1, 2, 3, 6, 8, 14, 15
- [32] Ying Li, Lingfei Ma, Zilong Zhong, Fei Liu, Michael A Chapman, Dongpu Cao, and Jonathan Li. Deep learning for lidar point clouds in autonomous driving: A review. *IEEE Transactions on Neural Networks and Learning Systems (TNNLS)*, 32(8):3412–3432, 2020. 1
- [33] Ze Liu, Han Hu, Yue Cao, Zheng Zhang, and Xin Tong. A closer look at local aggregation operators in point cloud analysis. In *European Conference on Computer Vision (ECCV)*, pages 326–342. Springer, 2020. 6
- [34] Ze Liu, Yutong Lin, Yue Cao, Han Hu, Yixuan Wei, Zheng Zhang, Stephen Lin, and Baining Guo. Swin transformer: Hierarchical vision transformer using shifted windows. In *IEEE/CVF International Conference on Computer Vision (ICCV)*, pages 10012–10022, 2021. 1, 2, 3, 15

- [35] Ilya Loshchilov and Frank Hutter. Decoupled weight decay regularization. *arXiv preprint arXiv:1711.05101*, 2017. 6
- [36] Tao Lu, Limin Wang, and Gangshan Wu. Cga-net: Category guided aggregation for point cloud semantic segmentation. In *Proceedings of the IEEE/CVF Conference on Computer Vision and Pattern Recognition*, pages 11693–11702, 2021. 14
- [37] Xu Ma, Can Qin, Haoxuan You, Haoxi Ran, and Yun Fu. Rethinking network design and local geometry in point cloud: A simple residual mlp framework. *International Conference on Learning Representations (ICLR)*, 2022. 1, 2, 3, 6, 7
- [38] Andres Milioto, Ignacio Vizzo, Jens Behley, and Cyrill Stachniss. Rangenet++: Fast and accurate lidar semantic segmentation. In *IEEE/RSJ International Conference on Intelligent Robots and Systems (IROS)*, pages 4213–4220, 2019. 2
- [39] Yatian Pang, Wenxiao Wang, Francis EH Tay, Wei Liu, Yonghong Tian, and Li Yuan. Masked autoencoders for point cloud self-supervised learning. *arXiv preprint arXiv:2203.06604*, 2022. 3
- [40] Chunghyun Park, Yoonwoo Jeong, Minsu Cho, and Jaesik Park. Fast point transformer. *IEEE/CVF Conference on Computer Vision and Pattern Recognition (CVPR)*, 2022. 1, 2, 3
- [41] Adam Paszke, Sam Gross, Francisco Massa, Adam Lerer, James Bradbury, Gregory Chanan, Trevor Killeen, Zeming Lin, Natalia Gimelshein, Luca Antiga, et al. Pytorch: An imperative style, high-performance deep learning library. *Advances in Neural Information Processing Systems (NeurIPS)*, 32, 2019. 2, 15
- [42] Charles R Qi, Hao Su, Kaichun Mo, and Leonidas J Guibas. Pointnet: Deep learning on point sets for 3d classification and segmentation. In *IEEE/CVF Conference on Computer Vision and Pattern Recognition (CVPR)*, pages 652–660, 2017. 1, 2, 3, 6, 7, 8, 14, 15
- [43] Charles Ruizhongtai Qi, Li Yi, Hao Su, and Leonidas J Guibas. Pointnet++: Deep hierarchical feature learning on point sets in a metric space. *Advances in Neural Information Processing Systems (NeurIPS)*, 30, 2017. 1, 2, 3, 6, 7
- [44] Guocheng Qian, Hasan Hammoud, Guohao Li, Ali Thabet, and Bernard Ghanem. Assanet: An anisotropic separable set abstraction for efficient point cloud representation learning. *Advances in Neural Information Processing Systems (NeurIPS)*, 34:28119–28130, 2021. 7
- [45] Guocheng Qian, Yuchen Li, Houwen Peng, Jinjie Mai, Hasan Abed Al Kader Hammoud, Mohamed Elhoseiny, and Bernard Ghanem. Pointnext: Revisiting pointnet++ with improved training and scaling strategies. *Advances in Neural Information Processing Systems (NeurIPS)*, 2022. 1, 2, 3, 6, 7, 8, 14, 15
- [46] Shi Qiu, Saeed Anwar, and Nick Barnes. Dense-resolution network for point cloud classification and segmentation. In *IEEE/CVF Winter Conference on Applications of Computer Vision (WACV)*, pages 3813–3822, 2021. 6
- [47] Shi Qiu, Saeed Anwar, and Nick Barnes. Geometric back-projection network for point cloud classification. *IEEE Transactions on Multimedia*, 24:1943–1955, 2021. 6
- [48] Shi Qiu, Saeed Anwar, and Nick Barnes. Semantic segmentation for real point cloud scenes via bilateral augmentation and adaptive fusion. In *IEEE/CVF Conference on Computer Vision and Pattern Recognition (CVPR)*, pages 1757–1767, 2021. 8, 15
- [49] Damien Robert, Bruno Vallet, and Loic Landrieu. Learning multi-view aggregation in the wild for large-scale 3d semantic segmentation. In *IEEE/CVF Conference on Computer Vision and Pattern Recognition (CVPR)*, pages 5575–5584, 2022. 8, 15
- [50] Haotian Tang, Zhijian Liu, Shengyu Zhao, Yujun Lin, Ji Lin, Hanrui Wang, and Song Han. Searching efficient 3d architectures with sparse point-voxel convolution. In *European Conference on Computer Vision (ECCV)*, pages 685–702, 2020. 2
- [51] Liyao Tang, Yibing Zhan, Zhe Chen, Baosheng Yu, and Dacheng Tao. Contrastive boundary learning for point cloud segmentation. In *IEEE/CVF Conference on Computer Vision and Pattern Recognition (CVPR)*, pages 8489–8499, 2022. 8, 14, 15
- [52] Lyne Tchapmi, Christopher Choy, Iro Armeni, JunYoung Gwak, and Silvio Savarese. Segcloud: Semantic segmentation of 3d point clouds. In *International Conference on 3D Vision (3DV)*, pages 537–547. IEEE, 2017. 14

- [53] Hugues Thomas, Charles R Qi, Jean-Emmanuel Deschaud, Beatriz Marcotegui, François Goulette, and Leonidas J Guibas. Kpconv: Flexible and deformable convolution for point clouds. In *IEEE/CVF International Conference on Computer Vision (ICCV)*, pages 6411–6420, 2019. 1, 2, 3, 6, 7, 8, 14, 15
- [54] Mikaela Angelina Uy, Quang-Hieu Pham, Binh-Son Hua, Thanh Nguyen, and Sai-Kit Yeung. Revisiting point cloud classification: A new benchmark dataset and classification model on real-world data. In *IEEE/CVF International Conference on Computer Vision (ICCV)*, pages 1588–1597, 2019. 2, 5, 6, 15
- [55] Ashish Vaswani, Noam Shazeer, Niki Parmar, Jakob Uszkoreit, Llion Jones, Aidan N Gomez, Łukasz Kaiser, and Illia Polosukhin. Attention is all you need. *Advances in Neural Information Processing Systems (NeurIPS)*, 30, 2017. 1, 2, 5
- [56] Wenhai Wang, Enze Xie, Xiang Li, Deng-Ping Fan, Kaitao Song, Ding Liang, Tong Lu, Ping Luo, and Ling Shao. Pyramid vision transformer: A versatile backbone for dense prediction without convolutions. In *IEEE/CVF International Conference on Computer Vision (ICCV)*, pages 568–578, 2021. 1, 2
- [57] Wenhai Wang, Enze Xie, Xiang Li, Deng-Ping Fan, Kaitao Song, Ding Liang, Tong Lu, Ping Luo, and Ling Shao. Pvt v2: Improved baselines with pyramid vision transformer. *Computational Visual Media*, 8(3):415–424, 2022. 1, 2
- [58] Yue Wang, Yongbin Sun, Ziwei Liu, Sanjay E Sarma, Michael M Bronstein, and Justin M Solomon. Dynamic graph cnn for learning on point clouds. *ACM Transactions On Graphics (TOG)*, 38(5):1–12, 2019. 1, 2, 3, 6, 7
- [59] Kan Wu, Houwen Peng, Minghao Chen, Jianlong Fu, and Hongyang Chao. Rethinking and improving relative position encoding for vision transformer. In *IEEE/CVF International Conference on Computer Vision (ICCV)*, pages 10033–10041, 2021. 5
- [60] Wenxuan Wu, Zhongang Qi, and Li Fuxin. Pointconv: Deep convolutional networks on 3d point clouds. In *IEEE/CVF Conference on Computer Vision and Pattern Recognition (CVPR)*, pages 9621–9630, 2019. 6
- [61] Zhirong Wu, Shuran Song, Aditya Khosla, Fisher Yu, Linguang Zhang, Xiaoou Tang, and Jianxiong Xiao. 3d shapenets: A deep representation for volumetric shapes. In *IEEE/CVF Conference on Computer Vision and Pattern Recognition (CVPR)*, pages 1912–1920, 2015. 2, 5, 6, 15
- [62] Tiange Xiang, Chaoyi Zhang, Yang Song, Jianhui Yu, and Weidong Cai. Walk in the cloud: Learning curves for point clouds shape analysis. In *IEEE/CVF International Conference on Computer Vision (ICCV)*, pages 915–924, 2021. 7
- [63] Chenfeng Xu, Bohan Zhai, Bichen Wu, Tian Li, Wei Zhan, Peter Vajda, Kurt Keutzer, and Masayoshi Tomizuka. You only group once: Efficient point-cloud processing with token representation and relation inference module. In *IEEE/RSJ International Conference on Intelligent Robots and Systems (IROS)*, pages 4589–4596. IEEE, 2021. 2
- [64] Mutian Xu, Runyu Ding, Hengshuang Zhao, and Xiaojuan Qi. Paconv: Position adaptive convolution with dynamic kernel assembling on point clouds. In *IEEE/CVF Conference on Computer Vision and Pattern Recognition (CVPR)*, pages 3173–3182, 2021. 6
- [65] Yifan Xu, Tianqi Fan, Mingye Xu, Long Zeng, and Yu Qiao. Spidercnn: Deep learning on point sets with parameterized convolutional filters. In *European Conference on Computer Vision (ECCV)*, pages 87–102, 2018. 6
- [66] Xu Yan, Chaoda Zheng, Zhen Li, Sheng Wang, and Shuguang Cui. Pointasnl: Robust point clouds processing using nonlocal neural networks with adaptive sampling. In *IEEE/CVF Conference on Computer Vision and Pattern Recognition (CVPR)*, pages 5589–5598, 2020. 6
- [67] Jianwei Yang, Chunyuan Li, Pengchuan Zhang, Xiyang Dai, Bin Xiao, Lu Yuan, and Jianfeng Gao. Focal self-attention for local-global interactions in vision transformers. *Advances in Neural Information Processing Systems (NeurIPS)*, 2021. 2
- [68] Lei Yang, Yanhong Liu, Jinzhu Peng, and Zize Liang. A novel system for off-line 3d seam extraction and path planning based on point cloud segmentation for arc welding robot. *Robotics and Computer-Integrated Manufacturing*, 64:101929, 2020. 1
- [69] Li Yi, Vladimir G. Kim, Duygu Ceylan, I-Chao Shen, Mengyan Yan, Hao Su, Cewu Lu, Qixing Huang, Alla Sheffer, and Leonidas Guibas. A scalable active framework for region annotation in 3d shape collections. *SIGGRAPH Asia*, 2016. 2, 5, 6, 7

- [70] Xumin Yu, Lulu Tang, Yongming Rao, Tiejun Huang, Jie Zhou, and Jiwen Lu. Point-bert: Pre-training 3d point cloud transformers with masked point modeling. *IEEE/CVF Conference on Computer Vision and Pattern Recognition (CVPR)*, 2022. **3**
- [71] Jinlai Zhang, Lyujie Chen, Bo Ouyang, Binbin Liu, Jihong Zhu, Yujin Chen, Yanmei Meng, and Danfeng Wu. Pointcutmix: Regularization strategy for point cloud classification. *Neurocomputing*, 505:58–67, 2022. **6**
- [72] Yang Zhang, Zixiang Zhou, Philip David, Xiangyu Yue, Zerong Xi, Boqing Gong, and Hassan Foroosh. Polarnet: An improved grid representation for online lidar point clouds semantic segmentation. In *IEEE/CVF Conference on Computer Vision and Pattern Recognition (CVPR)*, pages 9601–9610, 2020. **2**
- [73] Zhiyuan Zhang, Binh-Son Hua, and Sai-Kit Yeung. Shellnet: Efficient point cloud convolutional neural networks using concentric shells statistics. *IEEE/CVF International Conference on Computer Vision (ICCV)*, pages 1607–1616, 2019. **8, 15**
- [74] Hengshuang Zhao, Li Jiang, Chi-Wing Fu, and Jiaya Jia. Pointweb: Enhancing local neighborhood features for point cloud processing. In *IEEE/CVF Conference on Computer Vision and Pattern Recognition (CVPR)*, pages 5565–5573, 2019. **8, 15**
- [75] Hengshuang Zhao, Li Jiang, Jiaya Jia, Philip HS Torr, and Vladlen Koltun. Point transformer. In *IEEE/CVF International Conference on Computer Vision (ICCV)*, pages 16259–16268, 2021. **1, 2, 3, 5, 6, 7, 8, 9, 14, 15**
- [76] Xinge Zhu, Hui Zhou, Tai Wang, Fangzhou Hong, Yuexin Ma, Wei Li, Hongsheng Li, and Dahua Lin. Cylindrical and asymmetrical 3d convolution networks for lidar segmentation. In *IEEE/CVF Conference on Computer Vision and Pattern Recognition (CVPR)*, pages 9939–9948, 2021. **2**

Appendix

This appendix presents the per-category evaluations of the CDFormer with respect to recent state-of-the-art methods on Area 5 and 6-fold cross-validation of the S3DIS dataset for reference. Additionally, multiple visualization samples from both the S3DIS and ShapeNetPart datasets are presented to effectively demonstrate the proposed model’s effectiveness when compared to both the ground truth and baseline methods. Finally, the limitations of CDFormer are discussed.

A Additional Results on S3DIS

We present additional per-category evaluation results on both Area 5 and 6-fold cross-validation, as illustrated in Table 9 and 10. The results indicate that CDFormer demonstrates exceptional performance on large and flat categories such as *wall*, *beam*, and *column*. This can be attributed to the proposed collect-and-distribute mechanism, which facilitates the efficient capture of long-context information.

Table 9: Results of the proposed CDFormer and recent state-of-the-arts on Area 5 of S3DIS [3]. The **bold** and underline denote the first and second best performances.

Method	mIoU	mACC	OA	ceiling	floor	wall	beam	column	window	door	table	chair	sofa	bookcase	board	clutter
PointNet [42]	41.1	49.0	-	88.8	97.3	69.8	0.1	3.9	46.3	10.8	59.0	52.6	5.9	40.3	26.4	33.2
SegCloud [52]	48.9	57.4	-	90.1	96.1	69.9	0.0	18.4	38.4	23.1	70.4	75.9	40.9	58.4	13.0	41.6
PointCNN [31]	57.3	63.9	85.9	92.3	98.2	79.4	0.0	17.6	22.8	62.1	74.4	80.6	31.7	66.7	62.1	56.7
SPGraph [26]	58.0	66.5	86.4	89.4	96.9	78.1	0.0	42.8	48.9	61.6	84.7	75.4	69.8	52.6	2.1	52.2
PCT[19]	61.3	67.7	-	92.5	98.4	80.6	0.0	19.4	61.6	48.0	76.6	85.2	46.2	67.7	67.9	52.3
HPEIN [23]	61.9	68.3	87.2	91.5	98.2	81.4	0.0	23.3	65.3	40.0	75.5	87.7	58.5	67.8	65.6	49.4
MinkowskiNet [9]	65.4	71.7	-	91.8	98.7	86.2	0.0	34.1	48.9	62.4	81.6	89.8	47.2	74.9	74.4	58.6
KPConv [53]	67.1	72.8	-	92.8	97.3	82.4	0.0	23.9	58.0	69.0	81.5	91.0	75.4	75.3	66.7	58.9
CGA-Net[36]	68.6	-	-	94.5	98.3	83.0	0.0	25.3	59.6	71.0	92.2	82.6	76.4	77.7	69.5	61.5
CBL [51]	69.4	75.2	90.6	93.9	98.4	84.2	0.0	37.0	57.7	71.9	91.7	81.8	77.8	75.6	69.1	62.9
PointFormer [75]	70.4	76.5	90.8	94.0	98.5	86.3	0.0	38.0	63.4	74.3	89.1	82.4	74.3	80.2	76.0	59.3
PointNext-XL [45]	70.5	76.8	90.6	94.2	98.5	84.4	0.0	37.7	59.3	74.0	83.1	91.6	77.4	77.2	78.8	60.6
StratifiedFormer [25]	<u>72.0</u>	<u>78.1</u>	91.5	96.2	98.7	85.6	0.0	46.1	60.0	76.8	92.6	84.5	77.8	75.2	78.1	64.0
CDFormer	72.2	78.5	<u>91.2</u>	95.1	98.8	86.3	0.0	49.3	62.4	72.1	83.5	92.3	83.9	76.1	75.9	62.7

Table 10: Results on S3DIS [3] using 6-fold cross-validation. The **bold** and underline denote the first and second best performances. Note that * indicates additional 2D images are used and † indicates the reproduced result.

Method	mIoU	mACC	OA	ceiling	floor	wall	beam	column	window	door	table	chair	sofa	bookcase	board	clutter
PointNet [42]	47.6	66.2	78.6	88.0	88.7	69.3	42.4	23.1	47.5	51.6	54.1	42.0	9.6	38.2	29.4	35.2
RSNet [22]	56.5	66.5	-	92.5	92.8	78.6	32.8	34.4	51.6	68.1	59.7	60.1	16.4	50.2	44.9	52.0
SPG [26]	62.1	73.0	86.4	89.9	95.1	76.4	62.8	47.1	55.3	68.4	73.5	69.2	63.2	45.9	8.7	52.9
PointCNN [31]	65.4	75.6	88.1	94.8	97.3	75.8	63.3	51.7	58.4	57.2	71.6	69.1	39.1	61.2	52.2	58.6
PointWeb [74]	66.7	76.2	87.3	93.5	94.2	80.8	52.4	41.3	64.9	68.1	71.4	67.1	50.3	62.7	62.2	58.5
ShellNet [73]	66.8	-	87.1	90.2	93.6	79.9	60.4	44.1	64.9	52.9	71.6	84.7	53.8	64.6	48.6	59.4
RandLA-Net [21]	70.0	82.0	88.0	93.1	96.1	80.6	62.4	48.0	64.4	69.4	69.4	76.4	60.0	64.2	65.9	60.1
KPConv [53]	70.6	79.1	-	93.6	92.4	83.1	63.9	54.3	66.1	76.6	57.8	64.0	69.3	74.9	61.3	60.3
SCF-Net [16]	71.6	82.7	88.4	93.3	96.4	80.9	64.9	47.4	64.5	70.1	71.4	81.6	67.2	64.4	67.5	60.9
BAAF [48]	72.2	<u>83.1</u>	88.9	93.3	96.8	81.6	61.9	49.5	65.4	73.3	72.0	83.7	67.5	64.3	67.0	62.4
CBL [51]	73.1	<u>79.4</u>	89.6	94.1	94.2	85.5	50.4	58.8	70.3	78.3	75.7	75.0	71.8	74.0	60.0	62.4
PointFormer [75]	73.5	81.9	90.2	-	-	-	-	-	-	-	-	-	-	-	-	-
DeepViewAgg [49]*	74.7	-	-	90.0	96.1	85.1	66.9	56.3	71.9	78.9	79.7	73.9	69.4	61.1	75.0	65.9
PointNext-XL [45]	74.9	83.0	90.3	-	-	-	-	-	-	-	-	-	-	-	-	-
PointNext-XL [45]†	<u>74.9</u>	83.0	<u>90.3</u>	94.1	96.8	85.0	61.4	64.2	68.5	78.7	76.9	70.2	74.3	70.7	69.9	63.2
CDFormer	76.0	84.6	90.7	94.4	97.8	86.7	70.8	66.7	69.1	78.9	77.8	64.9	75.3	71.4	71.1	63.6

It is noteworthy that the Stratified Transformer proposed by [25] also leverages short- and long-range contexts in point cloud data, but takes advantage of a local window-based self-attention mechanism with shifted windows and the stratified sampling strategy. Despite sharing common ground with CDFormer, there are two fundamental differences between the two models. Firstly, the Stratified Transformer employs a window partitioning approach with local self-attention to model short-range relationships. This approach, however, is hindered by point clouds with varying densities, leading to complex and sophisticated designs and implementations to account for the differing number of points in each window. In contrast, CDFormer extracts local patches using the K nearest neighbor points and utilizes local self-attention to capture short-range information. This ensures that each local patch contains the same number of points and can be modeled directly by popular deep learning frameworks [1, 41], without the need for customized operators. Secondly, to capture long-range contexts, Stratified Transformer samples proximal points densely and remote points sparsely, using them as keys along with a shifted window strategy inspired by Swin Transformer [34]. The proposed CDFormer, in contrast, utilizes a collect-and-distribute mechanism that groups local patch features to a set of proxy reference points and exchanges information between them to capture long-range contexts, which are then distributed back to local points. Moreover, while Stratified Transformer has only been evaluated on segmentation tasks, CDFormer has been tested on both ModelNet40 [61] and ScanObjectNN [54] datasets for classification, demonstrating superior state-of-the-art performances.

B Visualization

To further demonstrate the superior performance of the proposed CDFormer, we provide additional visualizations on both S3DIS and ShapeNetPart datasets. Figure 7 illustrates the effectiveness of CDFormer in comparison with two baseline models, namely without the collect-and-distribute mechanism (**w/o CD**) and without context-aware position encoding (**w/o CAPE**). The results demonstrate that CDFormer with CD and CAPE achieves remarkable improvements, approaching the ground truth closely. Moreover, Figure 9 presents additional predictions by CDFormer, which exhibit exceptional ability in capturing short- and long-range contexts, and accurately segmenting complicated scenes.

Additionally, we illustrate visualizations of object part segmentations for multiple categories from the ShapeNetPart dataset in Figure 8. The predictions made by CDFormer are semantically accurate and closely resemble the ground truth, further validating the model’s effectiveness.

C Limitation

The proposed CDFormer performs well for object level recognition, both on CAD models in ModelNet40 [61] and real-world objects with challenging backgrounds in ScanObjectNN [54]. However, for 3D scene understanding, CDFormer has only been evaluated on indoor scenes from S3DIS [3],

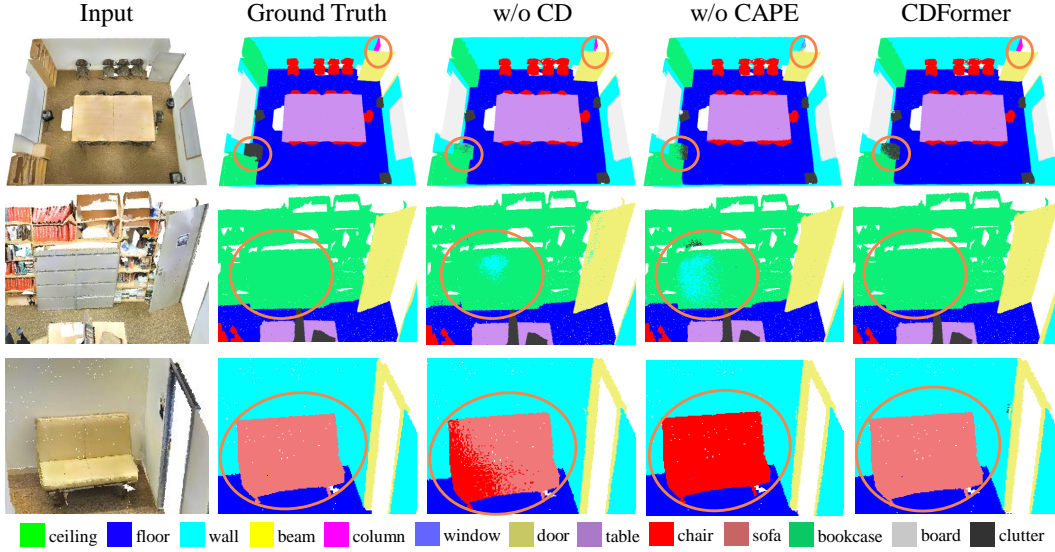


Figure 7: Visualizations of scene semantic segmentation on Area 5 of S3DIS by comparing CDFormer with its baselines and ground truth. The improved areas against baselines are highlighted by the orange circles.

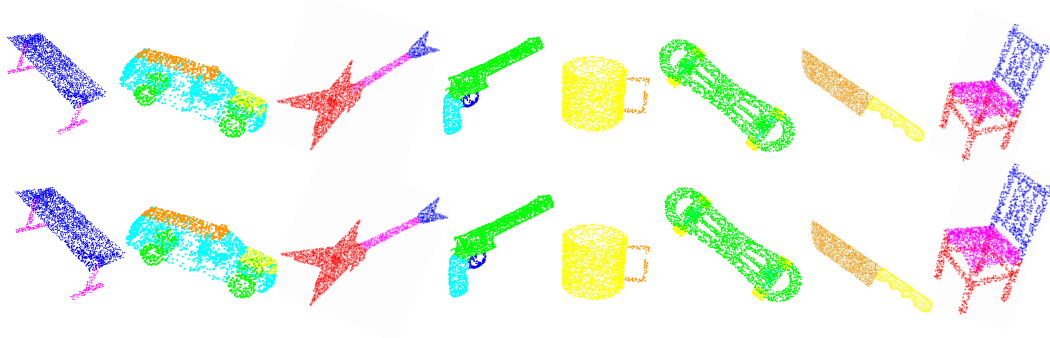


Figure 8: Visualizations of object part segmentation on multiple different categories from the ShapeNetPart dataset. The top row represents ground truth and the predictions from the proposed CDFormer are in the second row.

while outdoor scenes like SemanticKITTI [4] and NuScenes [6] have been ignored. These scenes pose new challenges, such as more points and sparser distribution of point clouds. We leave this as a topic for future work.

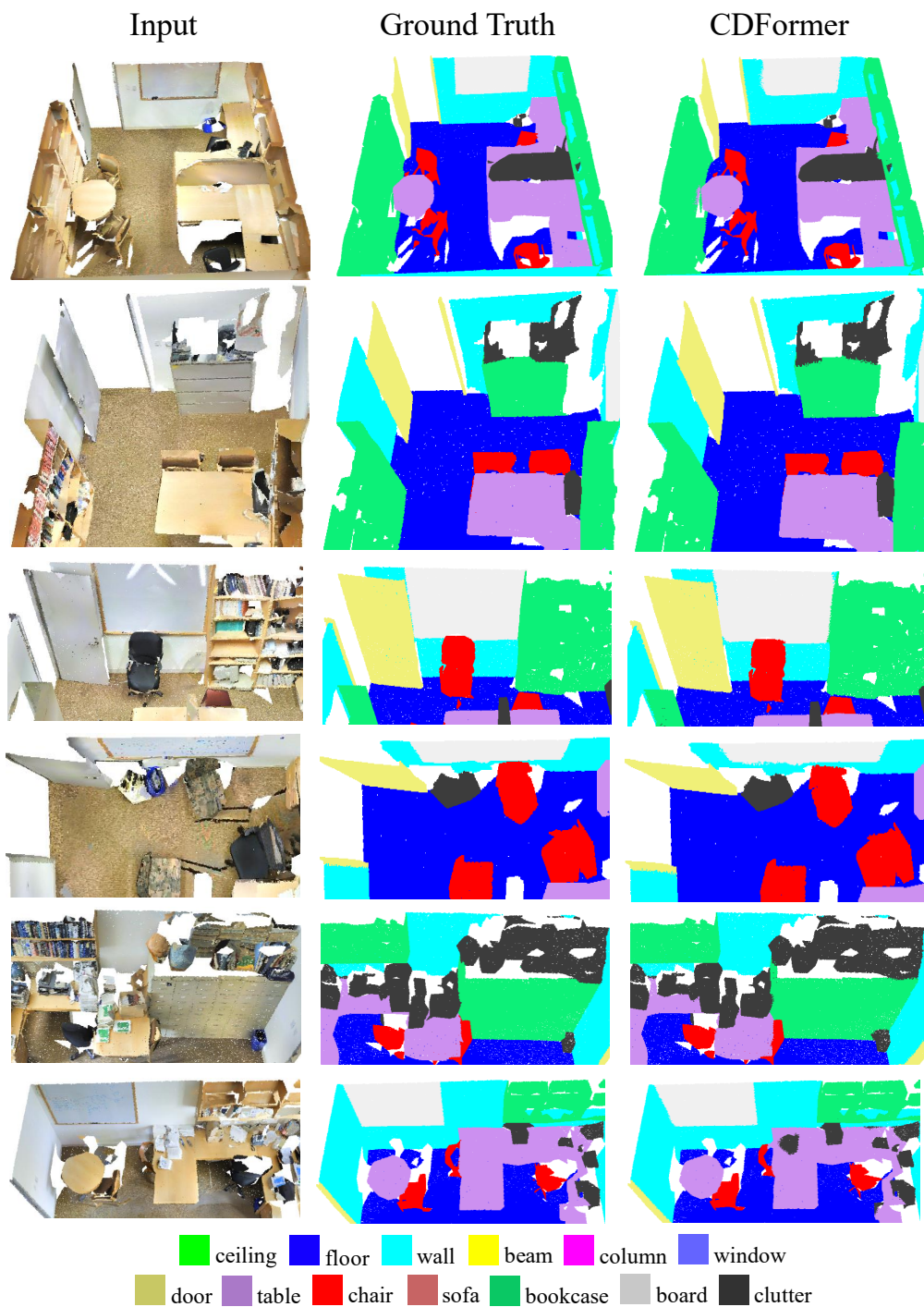


Figure 9: Visualizations of scene semantic segmentation on Area 5 of S3DIS by comparing CDFormer with the ground truth.